IEEE Access
Multidisciplinary | Rapid Review | Open Access Journal

Received May 21, 2020, accepted June 2, 2020, date of publication June 11, 2020, date of current version June 24, 2020.

Digital Object Identifier 10.1109/ACCESS.2020.3001756

A Clutter-Resistant SLAM Algorithm for Autonomous Guided Vehicles in Dynamic Industrial Environment

WEI WANG, YAOHUA WU, ZHENYU JIANG, AND JIAHUI QI
School of Control Science and Engineering, Shandong University, Ji'nan 250061, China
Corresponding author: Yaohua Wu (yaohua.wu@sdu.edu.cn)

ABSTRACT In dynamic and complicated industrial environments, feature-based SLAM based on laser scanner is a popular choice to achieve localization of autonomous guided vehicles. However, there are many clutters and dynamic objects degrading SLAM performance. This paper proposes a clutter-resistant SLAM solution where both point features generated from reflectors and line features are employed to improve SLAM robustness. First, a point feature recognition method based on geometrical characteristics of reflectors is developed to filter out clutters and identify true reflector landmarks; Then a dual-map based map management scheme is proposed for EKF-SLAM to further eliminate both types of fallacious landmarks and enhance its clutter resistance capability. The proposed methods eliminate adverse impact of clutters and thus improve SLAM performance in terms of accuracy, consistency and efficiency. The effectiveness of the proposed clutter-resistant SLAM solution is validated through real-time experiments. The absolute localization error is controlled within 19 mm and 31mm in X-axis and Y-axis respectively. The improved SLAM algorithm is proved to be accurate and efficient enough for practical application in dynamic and complicated industrial environments.

INDEX TERMS EKF, autonomous guided vehicle, SLAM, industrial environment.

I. INTRODUCTION

Simultaneous localization and mapping (SLAM) is a fundamental problem in the field of robotics research [1], which has been regarded as a ''holy grail'' [2]. A SLAM solution enables a mobile robot to incrementally build an environment map while localizing itself without any priori knowledge of the environment. Autonomous guided vehicle (AGV) is an important branch of mobile robots which is widely applied to transport heavy goods in industry [3]. The SLAM problem for AGV requires higher robustness and accuracy due to complicated and dynamic industrial environments and the demands for precise loading or unloading operation.

In the past thirty years, many notable achievements for SLAM problem have been obtained [4]–[7]. Scan matching is an effective method to solve SLAM problem [8], but it is not suitable for large scale scene due to high computational complexity. Estimation-theoretic approaches, based on Bayesian estimation framework, have been developed to solve SLAM problem [4], [9], [10]. Filtering-based algorithms have played an important role in SLAM solution, such as the extended Kalman Filter based SLAM (EKF-SLAM) [11], [12], noise-inclusive unscented Kalman filter based SLAM (UKF-SLAM) [13] and particle filter SLAM (FastSLAM) [14]. EKF-SLAM is the earliest approach and a number of derivative methods of which are developed to solve SLAM problems in indoor [12], outdoor [15], and underwater [16] environments. A novel method for online estimation of the input- and output-noise covariance matrices is proposed to improve convergency and stability of EKF-based localization [17], [18] and SLAM [11]. Reference [19] performs an EKF-based visual-inertial odometry to track the robot motion in SLAM process, where the optimized global map are fed back to the VIO to improve its accuracy. A point feature approach in [20] is recommended to lower computational complexity of EKF-SLAM. An invariant EKF-SLAM is proposed in [21] to achieve accurate map building in 1D/2D/3D scenarios, the accuracy is comparable to that of least square optimization based SLAM. Optimization-based algorithms consist of

The associate editor coordinating the review of this manuscript and approving it for publication was Christopher Kitts.

bundle adjustment [22] and pose-graph [23] etc., which have been widely applied in visual SLAM and are proved to have high consistency [24], [25].

SLAM in dynamic scenes is challengeable since dynamic objects may degrade SLAM performance. In visual SLAM, the dense information from images supports semantic segmentation to segment out movable objects in dynamic environments [26]–[28]. Sun *et al.* develop a motion removal approach and integrate it into the front end of RGB-D SALM, to detect dynamic objects during the RGB-D data pre-processing stage [29]. A deep learning method is applied for image semantic segmentation to reduce the interference of dynamic objects on the SLAM [30]. In [31], a dynamic deep learning SLAM is proposed for dynamic environments, in which a convolutional neural network is combined with multi-view geometry to identify dynamic objects. Dymczyk *et al.* develop a CNN classifier to recognize stable features on the basis of their expected lifetime [32]. Demim *et al.* point out that extraction often produces a high spatial uncertainty due to the sparse information of the raw laser LiDAR data compared to images, and they propose a new approach to filter features within a certain temporal window [33]. They also develop an adaptive SVSF-SLAM solution for dynamic environments, which can detect and remove dynamic parts of measurements [34]. In industrial environments with large size area, appearance-based maps are too large to handle [32] while sparse features are more suitable for SLAM solution, lowering computational complexity. Line features are widely employed for SLAM in many indoor scenes. Vakhitov *et al.* propose a learning method based on a fully-convolutional network to construct line segment descriptors [35]. However, in some dynamic industrial environments, line features may be unavailable in a short period of time when being occluded by some movable objects, e.g. forklifts and production materials. A stereo visual SLAM system is proposed in [36], which combines both points and line segments to enhance its robustness. Wang *et al.* also recommend a point-line feature based SLAM method [37], following which this paper also combines line features and point features to enhance the SLAM performance.

The point features generated from artificial reflectors are employed as secondary landmarks, to improve SLAM robustness in dynamic environments. The reflectors can be detected due to its property of reflecting laser beams with high intensity [38], [39]. However, there are some other substance, such as glass wall and metal racks with smooth surface, which can also reflect scattered laser beams in high quality. These substance can be identified as point features by mistaken. Besides, some unreliable line features are also generated in unstructured and cluttered industrial environments. All these unreliable features are known as ''fallacious landmarks'', which may have following adverse impacts on SLAM performance: first, fallacious landmarks may increase the difficulty of data association process and the probability of mismatching, which may cause divergence eventually; second, unstable features may generate inconsistent information when being observed at different positions or time, thus leading to more uncertainty and even divergence; third, excess fallacious landmarks may cause the computational complexity of EKF-SLAM increasing dramatically due to the higher dimension of covariance matrix.

The main purpose of this study is to present effective techniques for eliminating fallacious landmarks in cluttered industrial environments, which contributes to a better SLAM performance in terms of EKF convergency, accuracy and efficiency. The main contribution consists of two parts: first, a reflector landmark recognition method based on geometrical characteristics of reflectors is designed to identify true reflector landmarks during the sensor data pre-processing phase; second, referring to landmark management method in [40], a dual-map based EKF-SLAM framework is proposed. While a temporary map is maintained to filter out fallacious landmarks and generate candidate permanent landmarks, an official map is created to model the environment precisely.

The remainder of the paper is organized as follows. Section 2 presents a description of the mobile robot kinematic model, measurement model and the reflector landmark recognition method. Section 3 introduces the proposed dual-map based EKF-SLAM and the robust data association method. In section 4, the results of the proposed SLAM algorithm implemented in real industrial environment are presented and discussed. Section 5 draws conclusions and gives insights into future research.

II. MOBILE ROBOT SENSOR MODELS

A. MOTION MODEL

The robot state vector $X_r = \begin{bmatrix} x_r & y_r & \theta_r \end{bmatrix}^T$ is estimated at each discrete sampling instant k. In this study, a differential drive robot is used. The odometry information $u_r = \begin{bmatrix} d_l & d_r \end{bmatrix}^T$ is obtained from incremental wheel encoders, where d_l and d_r are the distance traveled by left and right wheels respectively. The robot motion model can be denoted as:

$$X_r(k+1) = f(X_r(k), u(k) + w(k)) \tag{1}$$

$$\begin{aligned} f(X_r(k), u(k)) &= \begin{bmatrix} x_r(k) \\ y_r(k) \\ \theta(k) \end{bmatrix} + \begin{bmatrix} \Delta x \\ \Delta y \\ \Delta\theta \end{bmatrix} \\ &= \begin{bmatrix} x_r(k) + \dfrac{d_r + d_l}{2} * \cos(\theta_r(k)) + \Delta\theta \\ y_r(k) + \dfrac{d_r + d_l}{2} * \sin(\theta_r(k)) + \Delta\theta \\ \theta_r(k) + \dfrac{d_r - d_l}{L} \end{bmatrix} \end{aligned} \tag{2}$$

where L is the wheelbase of robot, $w(k)$ represents the input noise and is modeled as Gaussian distribution with zero mean. The covariance matrix of $w(k)$ is defined as

$$Q(k) = \begin{bmatrix} \varepsilon^2 * d_l^2 + \gamma^2 & 0 \\ 0 & \varepsilon^2 * d_r^2 + \gamma^2 \end{bmatrix} \tag{3}$$

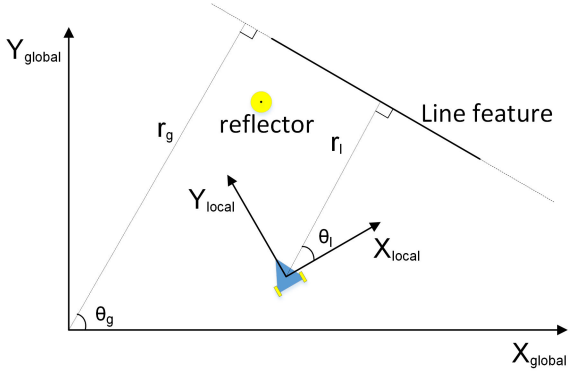

FIGURE 1. The line segment features and point features in global frame and local robot frame.

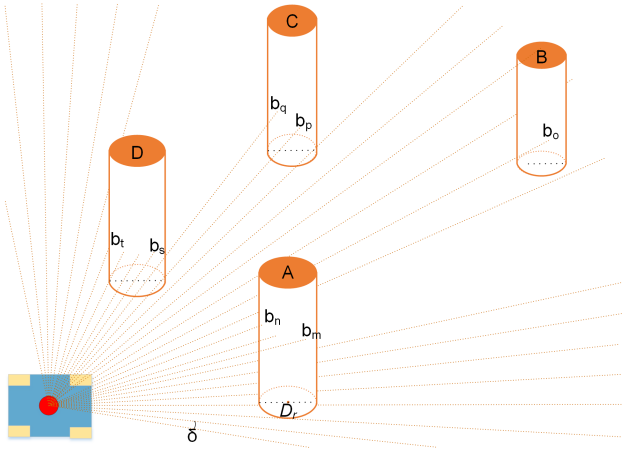

FIGURE 2. Reflector detected by laser beams.

where ε is the scale factor, indicating that the input uncertainty is proportional to the distance traveled. γ is added to compensate for the uncertainty of noise without movement.

B. MEASUREMENT MODEL

As shown in Fig. 1, two types of landmarks are employed in the proposed SLAM solution.

The line segment features can be denoted as polar coordinates:

$$X_l = \begin{bmatrix} r_{g,i} & \theta_{g,i} \end{bmatrix}^T, \quad i = 0, 1 \ldots n \tag{4}$$

The states of reflectors are recorded by cartesian coordinates in the global frame:

$$X_p = \begin{bmatrix} x_{g,i} & y_{g,i} \end{bmatrix}^T, \quad i = 0, 1 \ldots n \tag{5}$$

Despite the different forms of these two types of landmarks, the observation equation can be described in a centralized format as:

$$z(k) = h(X_r(k)) + v(k) \tag{6}$$

where $z(k)$ represents the observation at time k, and $h(X_r(k))$ is the measurement model with respect to robot state at time k. $v(k)$ describes the measurement noise with covariance matrix R.

This paper employs the split and merge algorithm for line feature extraction [41], since it can provide the end points of the extracted line segments incidentally. Then the least-squares method (LSQ) is employed for line fitting [11], to calculate line parameters in normal form:

$$x * \cos\theta_l + y * \sin\theta_l = r_l \tag{7}$$

where r_l is the distance from origin to the extracted line and θ_l denotes the angle between perpendicular and x-axis, in the local robot frame. The noise covariance matrix of line segment features R_l can be derived from the nominal values of laser sensor [11]. The measurement model in (6) for line features can be derived from transform equation as follows,

$$h_{l,i}(X_r(k)) = \begin{bmatrix} r_{g,i} - x_r * \cos\theta_{g,i} - y_r * \sin\theta_{g,i} \\ \theta_{g,i} - \theta_r \end{bmatrix}^T \tag{8}$$

Similarly, the measurement model $h(X_r(k))$ for point features is:

$$h_{p,i}(X_r(k)) = \begin{bmatrix} \sqrt{(x_{g,i} - x_r)^2 + (y_{g,i} - y_r)^2} \\ \arctan\dfrac{y_{g,i} - y_r}{x_{g,i} - x_r} - \theta_r \end{bmatrix}^T \tag{9}$$

C. POINT FEATURE EXTRACTION

1) LASER BEAMS CLUSTERING

Fig. 2 illustrates how the laser scanner perceive the environment, where there are four reflectors in the robot's field of view. As shown in the figure, D_r is the diameter of the reflectors which is 80mm, whereas δ is the angular resolution of laser beams from the laser scanner. The laser beams are indexed by m, n, o, etc.

Usually, the reflectors can be detected based on their strong reflective properties. However, we cannot ignore the fact that some materials can also reflect laser beams with high intensity, which may cause false positive detection. Most existing methods for reflector recognition are based on the priori known position of reflectors in the map [42], [43]. In SLAM process, the landmark position information is unknown, which imposes extra difficulty on recognizing true reflectors from clutters. The reflector detection method proposed in this paper is rigorous, and it considers more complicated situation, which is introduced in Algorithm 1.

In step 1, we select all the laser beams in a scan cycle which are reflected with high intensity. A series of consecutive laser beams (e.g. $\{b_m \ \ldots \ b_n\}$ in Fig. 2) are divided into a cluster C_j.

The consecutive laser beams in a cluster collected in step 1 may come from different objects. For instance, laser beams $\{b_p \ldots b_t\}$ hit different reflectors but are gathered in the same cluster. This may happen occasionally when these objects are detected by laser scanners from a special point of view. Therefore, a mean error analysis method (MEA) is proposed in step 2 to determine whether laser beams in a cluster are from a single object. The MEA method calculates the

Algorithm 1 Reflector Extraction

Input:
D_r;
laser beam measurements b_i, $i \in [1, 720]$;
Output:
Relative reflector positions, $\{(d_p, \theta_p)_j\}$;
1: Find laser beam clusters $\{C_j\}$ that may come from reflectors based on reflection intensity;
2: Use the MEA method to determine whether each cluster comes from a single object;
3: Identify clusters that come from reflectors based on its geometrical property;
4: Calculate relative reflector positions $\{(d_p, \theta_p)_j\}$;
5: **return** $\{(d_p, \theta_p)_j\}$;

mean measurement distance of laser beams in a cluster, and then the mean error of these measurement distance from the mean value is obtained. If the mean error is less than the pre-determined threshold τ_e, the laser beams in the cluster are reflected by a single object. Otherwise, the cluster should be reallocated according to the measurement distance of each laser beam in the cluster. In general, the mean error should be less than the half of reflector radius if all laser beams are from a single reflector. Based on this, we empirically set the value of τ_e as 30mm.

In step 3, a reflector recognition method is developed to determine whether laser beams in each cluster C_j are reflected by a reflector. The recognition method is based on the geometrical characteristics of reflectors and is described in detail in next subsection.

In step 4, the relative positions of all the identified reflectors are calculated, as well as the noise covariance matrix.

2) REFLECTORS RECOGNITION

Generally, reflectors can reflect a number of consecutive laser beams while the cluttered substance can only reflect sparse laser beams occasionally. Taking an example of reflector A, which is hit by laser beams $\{b_m \dots b_n\}$, the recognition method is described as follows.

The number of the laser beams hit onto the reflector is negatively proportional to the observation distance. The minimum number of laser beams N_{min} that hit the reflector can be calculated even though the number in practical may be higher than N_{min}. First, the shortest distance between the laser scanner and the edge of reflector d is obtained by (10), then N_{min} is calculated by (11).

$$d = \frac{\sum_{i=m}^{n} d_i}{n - m + 1} \tag{10}$$

$$N_{min} = \lfloor \frac{D_r}{2\sin(\frac{\delta}{2}) * d} \rfloor \tag{11}$$

where d_i is the measurement distance of laser beam b_i, and the operator $\lfloor \cdot \rfloor$ denotes the lower integer bound. Based on this restriction, an observed object is recognized as an available reflector landmark only if the number of detected laser beams satisfy: $n - m + 1 \geq N_{min}$. Once a reflector landmark is identified, the polar coordinates of the reflector landmark (d_p, θ_p) in the local robot frame can be calculated approximately as follows:

$$d_p = d + \frac{D_r}{2} \tag{12}$$

$$\theta_p = \frac{\sum_{i=m}^{n} \theta_i}{n - m + 1} \tag{13}$$

where θ_i is the angle of b_i. The noise covariance matrix R_p can be obtained by (14),

$$R_p = \begin{bmatrix} \frac{1}{\sigma^2}(n - m + 1) & 0 \\ 0 & (\frac{1}{4}\delta(n - m + 2))^2 \end{bmatrix} \tag{14}$$

where σ denotes the standard deviation of range measurement uncertainty for laser beams.

III. DUAL-MAP BASED EKF-SLAM ALGORITHM

A. EKF-SLAM

The SLAM problem comprises two main subproblems: robot localization and environment mapping. In EKF-based SLAM, a state vector X, consisting of 2-D robot position and landmark positions, is employed to record estimation results:

$$X = \begin{bmatrix} X_r & X_l & X_p \end{bmatrix}^T \tag{15}$$

Besides, the covariance matrix P is also computed to describe the estimation uncertainty and correlation between the states of the robot and landmarks, which consists of four blocks,

$$P = \begin{bmatrix} P_{r,r} & P_{r,m} \\ P_{m,r} & P_{m,m} \end{bmatrix}^T \tag{16}$$

where $P_{r,r}$ denotes the uncertainty of robot state estimation and $P_{m,m}$ represents estimation uncertainty of landmark positions. $P_{r,m}$ and its transpose $P_{m,r}$ are the cross-covariance matrices which represent correlation between the robot state estimation and landmark state estimation.

1) PREDICTION STEP

In the prediction step, the state of robot at current sampling instant k is estimated and denoted as $\widetilde{X}(k)$ on the basis of posterior robot state estimate $X(k-1)$ and odometer information. The covariance matrix is updated correspondingly, while landmarks remain stationary.

$$\begin{aligned} \widetilde{X}(k) &= f(X(k-1), u(k-1)) \\ &= \begin{bmatrix} f_r(X_r(k-1), u(k-1)) \\ X_l(k-1) \\ X_p(k-1) \end{bmatrix} \\ \widetilde{P}(k) &= \begin{bmatrix} \widetilde{P}_{r,r}(k) & \widetilde{P}_{r,m}(k) \\ \widetilde{P}_{m,r}(k) & \widetilde{P}_{m,m}(k) \end{bmatrix} \end{aligned} \tag{17}$$

$$= \begin{bmatrix} F_X P_{r,r}(k-1) F_X^T + F_u Q(k-1) F_u^T & F_X P_{r,m}(k-1) \\ P_{m,r}^T(k-1) F_X^T & P_{m,m}(k-1) \end{bmatrix} \tag{18}$$

f_r gives a prediction for robot pose according to (2), whereas F_X and F_u are the jacobian matrices of f_r with respect to X_r and u.

2) CORRECTION STEP

Supposing that data association is completed, the main objective of the correction step is twofold: First, to update the state of robot and landmarks, as well as the covariance matrix, on the basis of paired observations; Second, to append newly observed landmarks to the global map.

The observed landmarks at time instant k are denoted by $z(k) = \left[z_M(k)\ z_N(k) \right]^T$, where $z_M(k)$ represents paired landmarks list, and $z_N(k)$ is the newly observed landmarks list which have never been observed before. Assume that the i^{th} landmark in $z_M(k)$ is paired with j^{th} landmark in global map, then the innovation of the observed landmark i can be derived from (19), considering a centralized form of both line segment features and cylinder reflectors.

$$v_j(k) = z_{M_i}(k) - h_j(X_r(k)) \tag{19}$$

Then the posterior system state and the covariance matrix can be updated in batch as follows:

$$S(k) = H(k)\widetilde{P}(k)H^T(k) + R(k) \tag{20}$$
$$K(k) = \widetilde{P}(k)H^T(k)S^{-1}(k) \tag{21}$$
$$X(k) = \widetilde{X}(k) + K(k)V(k) \tag{22}$$
$$P(k) = \widetilde{P}(k) - K(k)S(k)K^T(k) \tag{23}$$

where $H(k)$ is the jacobian matrix of $h(X_r(k))$ (see (8) or (9)) with respect to $\widetilde{X}_r(k)$ and $z_M(k)$, according to the type of the paired landmarks. $K_j(k)$ is the Kalman gain.$V(k)$ denotes the innovation matrix which is composed of $v_j(k)$ for all paired landmarks.

Then the newly observed landmarks $z_N(k)$ should be added to the global map, by appending the state vector. The covariance matrix is also upgraded. First, the landmarks coordinates in global frame should be derived from that in local robot frame through coordinates transformation. The coordinates transformation formulas of the line segment features $g_l(\cdot)$, and reflector landmarks $g_p(\cdot)$ are given by (24) and (25) respectively.

$$\begin{aligned} X_l &= \begin{bmatrix} r_g & \theta_g \end{bmatrix}^T = g_l(r_l, \theta_l) \\ &= \begin{bmatrix} x_r\cos(\theta_l + \theta_r) + y_r\sin(\theta_l + \theta_r) + r_l \\ \theta_l + \theta_r \end{bmatrix} \end{aligned} \tag{24}$$

$$\begin{aligned} X_p &= \begin{bmatrix} x_g & y_g \end{bmatrix}^T = g_p(d_p, \theta_p) \\ &= \begin{bmatrix} x_r + d_p\cos(\theta_p + \theta_r) \\ y_r + d_p\sin(\theta_p + \theta_r) \end{bmatrix} \end{aligned} \tag{25}$$

The state vector is augmented by (26):

$$X_p = \begin{bmatrix} X(k) & X_{l,new} & X_{p,new} \end{bmatrix}^T \tag{26}$$

where $X_{l,new}$ and $X_{p,new}$ are newly observed landmark lists which are transformed into the global frame through (24) and (25). The covariance matrix can be augmented as shown in Fig. 3, where:

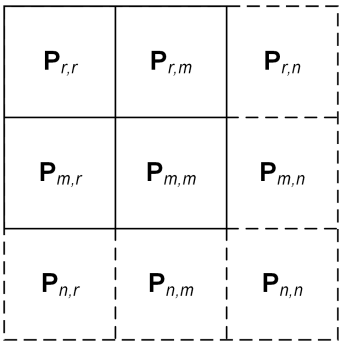

FIGURE 3. The augment of system covariance matrix.

$$P_{r,n} = P_{r,r}G_X^T(k) \tag{27}$$
$$P_{m,n} = P_{r,m}G_X^T(k) \tag{28}$$
$$P_{n,r} = P_{r,n}^T \tag{29}$$
$$P_{n,m} = P_{m,n}^T \tag{30}$$
$$P_{n,n} = G_X(k)P_{r,r}G_X^T(k) + G_z(k)R(k)G_z^T(k) \tag{31}$$

$G_X(k)$ and $G_z(k)$ are jacobian matrices of $g_l(X(k)$ or $g_p(X(k)$ (according to the type of the observation) with respect to the robot pose and the observation.

B. DATA ASSOCIATION

Data association aims to match the currently observed features with existed landmarks in the global map. An accurate data association is required to achieve high-quality SLAM. Otherwise, poor SLAM performance with low accuracy and consistency may be obtained, even divergence. This paper presents an efficient data association method to realize real-time SLAM.

For each currently observed landmark $z_i(i = 0, 1 \ldots m)$ in $z(k)$, the data association process can be described as follows:

1) Find all landmarks in the global map which are the same type as z_i.
2) Calculate Euclidean distance between each of them and z_i, and then select 5 nearest landmarks as pairing candidates.
3) Calculate Mahalanobis distance D between each of these five candidates and z_i, according to (32).

$$D = (h_j - z_i)^T S^{-1}(h_j - z_i) \tag{32}$$

where h_j is calculated through (8) or (9) for j^{th} landmark in the global map, and S can be derived from (20).

4) Compare the minimum Mahalanobis distance D_{min} with a predetermined threshold τ_d. If $D_{min} > \tau_d$, the pairing for z_i is failed, thus the observed landmarks z_i is defined as a newly observed landmark. Conversely, if $D_{min} < \tau_d$, the corresponding landmark Z_{pair} in the global map is paired with z_i. Note that the value of τ_d is

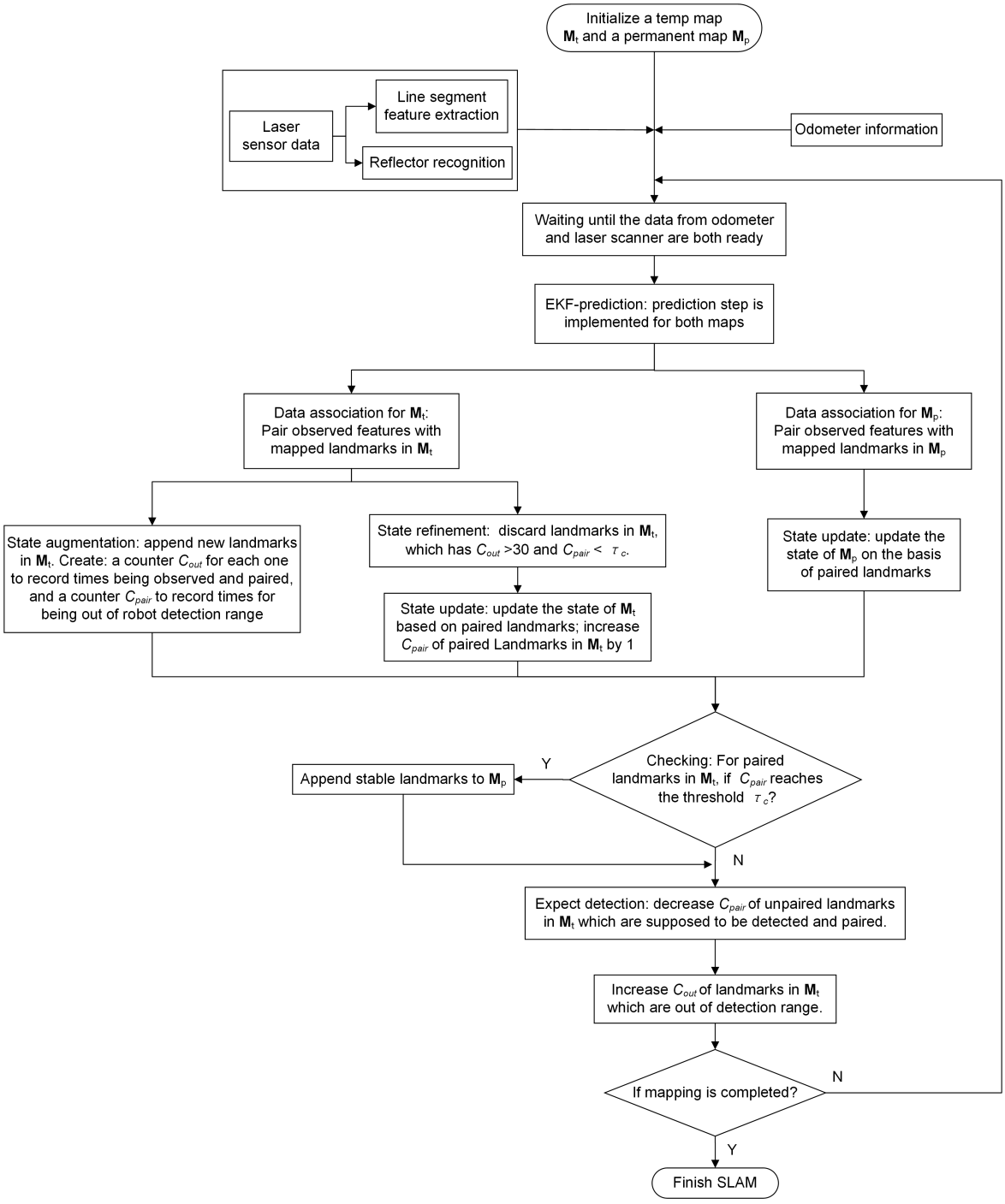

FIGURE 4. The SLAM solution with dual-map based map management scheme.

determined empirically by conducting massive tests in practical environments, and we suggest that this should be implemented before applying this method in other environments.

5) However, if Z_{pair} has been previously paired with other currently observed landmarks, then the Mahalanobis distance of these two pairs should be compared. The one with minimum Mahalanobis distance will be matched with Z_{pair} eventually, while the other observed landmark will be discarded.

Once the matching process for all the currently observed landmarks are completed, a joint compatibility for these

pairings and robot position estimation is calculated referring to [44], to make sure whether they are jointly compatible with each other. The result is examined by χ^2 test with confidence level α. The main objective is to reduce the possibility of accepting spurious pairings, since the prediction and measurement errors are correlated.

C. DUAL-MAP BASED EKF-SLAM

As mentioned above in section 2.3.2, the proposed landmark recognition method can only eliminate a portion of fallacious reflector landmarks. This section presents a dual-map based map management scheme to further exclude both fallacious point features and line features. Fig. 4 gives the flowchart of the proposed dual-map based EKF-SLAM, and the process is illustrated in detail as follows.

In the initialization step, a temporary map M_t and a permanent map M_p are initialized, supposing that both coordinate frames are aligned with the starting pose of robot, the initial covariance matrix P_0 is also set.

Once the SLAM process starts, the odometer and laser sensor data are received and processed consecutively. The line segment features are extracted through split and merge method and the LSQ algorithm, whereas reflector landmarks are identified through the proposed point feature recognition method in section 2.3.

Once all the sensor data are ready, EKF algorithm is implemented. For both maps M_t and M_p, the prediction step is implemented in the same manner. The robot state and the covariance matrix for state estimation are predicted.

Then the data association process is implemented for both maps, and the pairing results are used for correction step. As for the permanent map M_p, unpaired observations will be neglected, while paired observations are used for correction step. In temporary map, unpaired observations are appended as new landmarks. Each new landmark in M_t is initialized with a counter C_{pair}, to record the frequency that it is observed and paired. Another counter C_{out} is also set to record the number of times that the landmark is out of the robot detection reange. On the other hand, the landmark which has $C_{out} > 30$ and $C_{pair} < \tau_c$ is thought to be redundant and is removed from M_t. These landmarks are identified as fallacious landmarks since they have been out of robot detection range already. Discarding these landmarks in M_t considerably reduces computational complexity and the possibility of mismatching in data association process. The posterior state of M_t is estimated on the basis of paired landmarks, where a virtual robot state is also updated to support EKF algorithm for M_t. For all the landmarks that are paired with current observations, their counters C_{pair} are increased by 1. The counters C_{pair} of all paired landmarks in M_t are checked. If C_{pair} of a landmark exceeds the threshold τ_c and it has not been added to M_p, then the landmark is identified as a stable landmark which should be included in M_p for system state correction. Appending stable landmarks to M_p instead of removing fallacious landmarks from M_p may effectively avoid unreliable information generated by these fallacious landmarks. It is worth mentioning that an appropriate value of τ_c should be selected, to ensure that newly observed true landmarks can be included in the permanent map within a reasonable time period, while rejecting almost all the fallacious landmarks. Motivated by this purpose, we conduct numerous experiments to determine the value of τ_c.

FIGURE 5. Platform used in the experiment.

To improve the reliability of C_{pair}, further inspection is performed over the landmarks in the temporary map M_t. Normally a landmark in M_t is supposed to be detected when it is in the robot detection range, whereas the detection range of the robot is pre-defined by radius r_0 but not the maximum perceptual range. However, if this landmark is not paired with any observation, its counter C_{pair} should be decreased by 1. In this way, unreliable landmarks are less likely to be added to the permanent map. On the contrary, if any landmark in the temporary map M_t is out of robot detection range, the counter C_{out} is increased by 1.

IV. EXPERIMENTAL RESULTS

The effectiveness of the proposed landmark recognition method and dual-map based EKF-SLAM solution are validated through practical experiments in a manufacturing factory, which spans an area of approximately $82.5 \times 52\ m^2$ with complex components such as autonomous devices, storage racks and an office etc. The platform used in the experiments is shown as Fig. 5-a, which is a simple-assembled vehicle equipped with a laser scanner (Fig. 5-b).

The experiments are carried out in an industrial PC with a 2.8 GHz Intel Core i7 processor, and the algorithm is executed by using C#. The values of some basic parameters are given in Table 1.

First, the reflector parameter extraction method is tested. In the experiment, a reflector is observed by the laser scanner at different distance. For each distance value, the measurement results are obtained by measuring the reflector at 10 different orientations of the vehicle. The results in Table 2 show the approximation error of reflector parameter extraction. Generally, the measurement error is not very high and increases slightly with the reflected number of

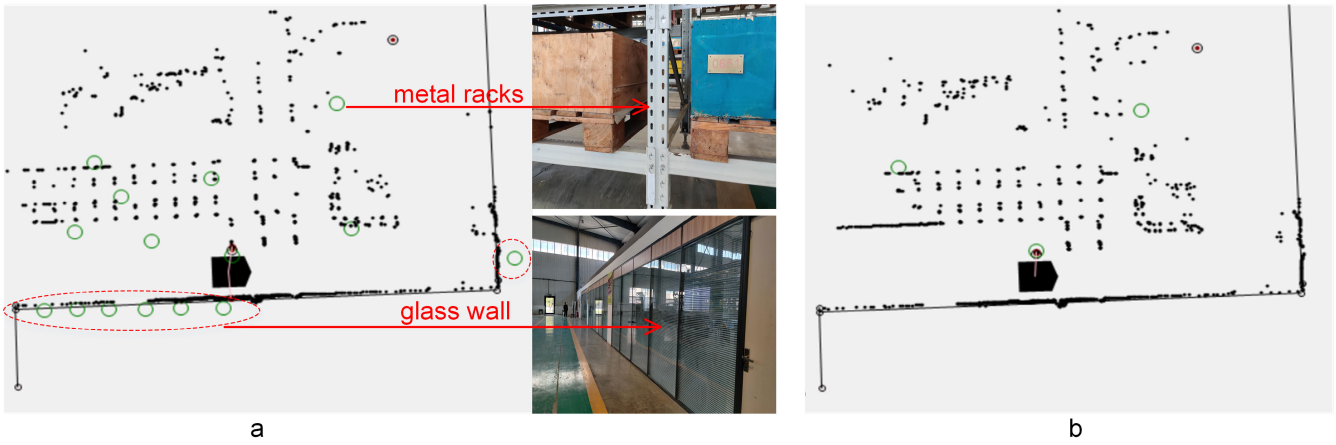

FIGURE 6. Landmark recognition results.

TABLE 1. Value of system parameters in the experiments.

Parameters	Values
ε	0.15
δ	0.5°
γ	0.5mm
τ_c	150
τ_e	30mm
r_0	50mm
τ_d	400mm
α	0.01mm
σ	20mm
P_0	$\begin{bmatrix} 0 & 0 & 0 \\ 0 & 0 & 0 \\ 0 & 0 & 0 \end{bmatrix}$

TABLE 2. Reflector parameter extraction results.

Distance (m)	Number of reflected laser beams	Average measurement distance (m)	measurement error (m)	standard error (m)
1	8	1.015	0.015	0.0029
1.5	5	1.513	0.013	0.0035
2	4	2.012	0.012	0.0033
2.5	3	2.51	0.01	0.004
3	2	3.011	0.01	0.0044
4	1	4.011	0.011	0.0054
5	1	5.007	0.007	0.0056
10	1	10.018	0.018	0.0069

laser beams, and this may be attributable to the geometrical property of reflectors. On the other hand, the standard error increases with the measuring distance.

Then we implement the reflector recognition method and the results are shown in Fig. 6. The raw point cloud of the laser sensor is described by black dots. The black circles represent the true position of reflector landmarks, whereas the green circles show the reflector landmarks detected by laser scanner. The true positions of these reflectors are measured manually through reliable mechanical method. We use some accurate tools such as handheld laser rangefinders, laser levels, and square rulers etc., and we obtain the final

FIGURE 7. Reflector landmarks in the warehouse.

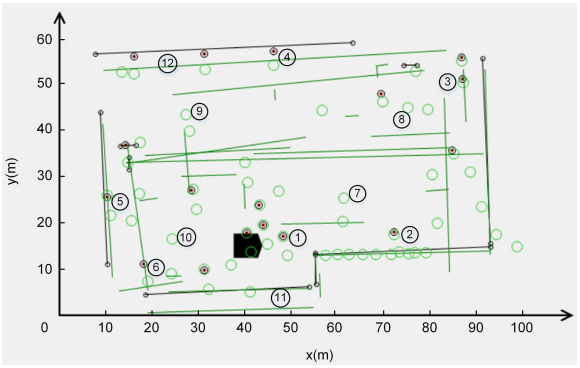

FIGURE 8. Feature map with "fallacious landmarks" built by standard EKF-SLAM.

measurement results as an average of 10 repeats. Fig. 6-a shows the detection results where only substance reflectivity are utilized, while Fig. 6-b illustrates the performance of the proposed reflector recognition method. We can see that there are numerous fallacious landmarks in Fig. 6, caused by some substance with high reflectivity. Many of them originate from metal racks or other metal materials with smooth surface as shown in the figure. Notice that there are a row of fallacious landmarks around the line feature, as highlighted by a dotted ellipse. These fallacious landmarks are generated from a glass wall of an office in the factory, which promiscuously reflects

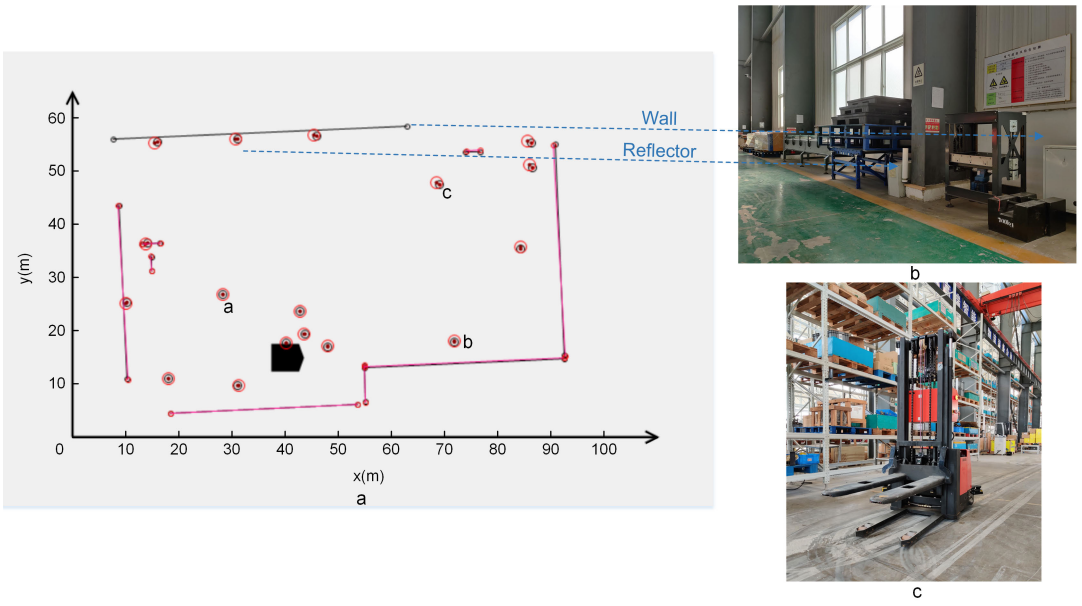

FIGURE 9. Feature map built by proposed SLAM algorithm.

FIGURE 10. Possible fallacious line segment landmarks.

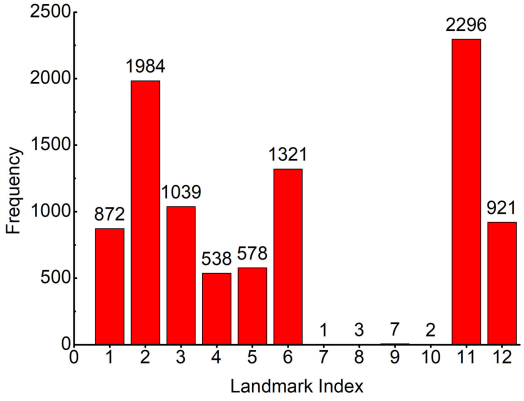

FIGURE 11. The frequency of landmarks being observed and paired.

laser beams with high intensity. In Fig. 6-b, it can be seen that most fallacious landmarks are eliminated except for those caused by faraway clutters. This is mainly because that N_{min} derived from (11) for faraway reflectors are equal to 1, which coincides with the fact that clutters always reflect single laser beam. However, the faraway fallacious landmark marked by a dotted circle at the most right side in Fig. 6-a, which disappears in Fig. 6-b, is not filtered out by the landmark recognition method, but because that it is not detected at this observation. This is due to the fact that there are more uncertainties of faraway clutters due to angular resolution of laser beams.

The following experiments are implemented in the storage warehouse of a factory, where reflectors are deployed at some key positions in the warehouse as shown in Fig. 7. Both the proposed SLAM algorithm and the standard EKF-SLAM are implemented, and their performance are compared in detail. The robot starts from a position which is defined as the origin of the global frame. It travels counterclockwise around a loop path and performs the SLAM process until it returns to somewhere close to the start position.

The true locations of landmarks are measured manually through reliable mechanical method. Fig. 8 shows the temporary map, which is the result of standard EKF-SLAM, whereas the permanent map is illustrated in Fig. 9. The true positions of reflector landmarks and line segment landmarks are represented by black circles and line segments respectively. The landmarks in temporary map are described by green circles and line segments, whereas the red circles and line segments represent landmarks in permanent map. From Fig. 8 we see that the temporary map comprises a large number of fallacious landmarks, including those removed from M_t which have $C_{out} > 30$ and $C_{pair} < \tau_c$ since they have already brought adverse impact on the map building. As for the fallacious line segment landmarks, some of them are caused by two or more planes which are close to each other as shown in Fig. 10-a. They are merged into a single line when being observed from a special point of view. Another

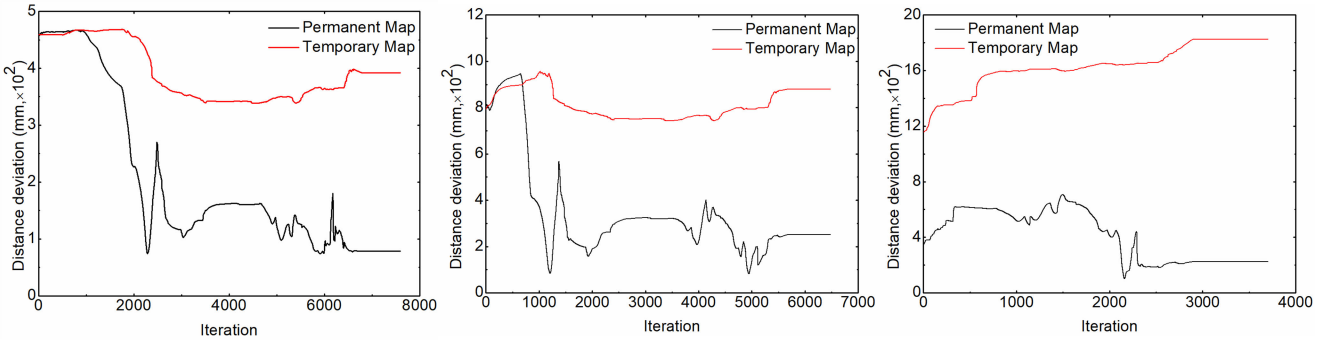

FIGURE 12. The estimated distance error of three reflector landmarks in both maps.

source of fallacious line segment landmarks comes from the objects that are not on the robot's horizontal observing plane (see Fig. 10-b). They can be detected occasionally as a result of fluctuating observing plane of the robot when it runs on uneven ground. All the inaccurate information that originates from these fallacious landmarks may affect mapping performance adversely. Fortunately, it can be seen in Fig. 9 that all the fallacious landmarks caused by clutters in the current environment are eliminated by the proposed methods. Most of fallacious point features are filtered out by the reflector recognition method, and the dual-map based scheme eliminates the rest fallacious point features and line segment features thoroughly. Furthermore, most of real landmarks in the temporary map deviate from their true locations considerably, while the landmarks position deviation in the generated permanent map is relatively negligible. This is largely attributable to the fact that uncertainties and inaccurate information generated by fallacious landmarks are eliminated.

Notice that a line segment landmark on the top of Fig. 9 is not included in the permanent map. This is the result of the dynamic environment. The reason is that the related wall in real environment is blocked and split into several pieces by other temporarily placed objects as shown in Fig. 9-b. These small pieces of line segments are not recognizable due to the threshold set for the line extraction method. There are various other dynamic objects like forklifts (Fig. 9-c), and even workers which may cause obstruction. That's the most important reason that we introduce stable reflectors as auxiliary landmarks to constitute the environment map. Besides, the combination of multiple landmarks makes it easier to find a balance of the trade-off introduced by [40], where an appropriate number of landmarks can always be determined.

In Fig. 11, the frequency that reflector landmarks 1-6, fallacious landmarks 7-10, and line segment landmarks 11 and 12 in Fig. 8 being observed and paired successfully are illustrated. Normally, real landmarks are detected frequently and permanently, generally much more than 100 times. On the contrary, fallacious landmarks can be observed occasionally. Therefore the C_{pair} of these landmarks are always maintained at a considerably low level. Another reason is that the C_{pair} of fallacious landmarks are rigorously controlled by the expect

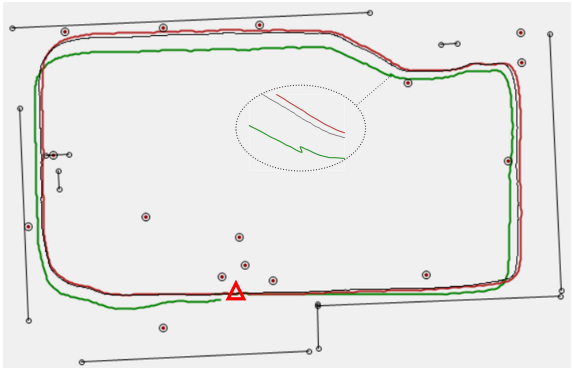

FIGURE 13. Estimated trajectories of robots by two different SLAM algorithms.

observation step. Therefore, the fallacious landmarks barely have opportunities to be added into permanent map.

To further analyze how the mapping accuracy is improved by the proposed SLAM algorithm, the position deviation of landmarks a, b, and c in Fig. 9-a from true locations in these two maps are illustrated in Fig. 12. It is obvious that landmark position deviation in the temporary map fluctuates at a high level, while the landmark position estimation in permanent map all converge to their true locations. This demonstrates that eliminating fallacious landmarks in cluttered industrial environment may improve mapping accuracy to a large extent. Our proposed methods are worth studying and have significant implications for practical SLAM in industrial environments.

The robot localization accuracy in the SLAM process is another key metrices for evaluating SLAM performance. As mentioned above, our proposed SLAM algorithm updates robot pose in both temporary map and permanent map independently. Fig. 13 illustrates the accuracy of robot trajectories generated by the proposed SLAM algorithm (red line) and the standard EKF-SLAM (green line). The ground truth (black line) is obtained from a localization solution provided by SICK, which is validated to be reliable but expensive, and has been extensively applied in industry. The start position is approximately labeled by a red triangle in the image. The result shows that the robot trajectory from

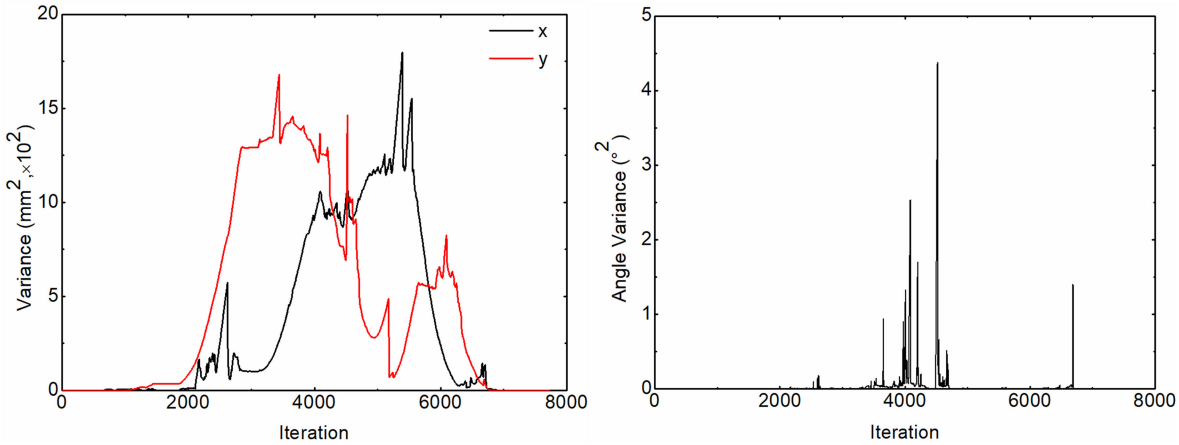

FIGURE 14. Estimated position and orientation variance of robot by the proposed SLAM algorithm.

the proposed SLAM approaches the ground truth closely, while the trajectory from the standard EKF-SLAM deviates from the ground truth gradually. This coincides with the fact that more and more unstable fallacious landmarks are included in the temporary map and the adverse impact generated by these fallacious landmarks accumulates during the SLAM process.

On the other hand, the proposed SLAM solution also improves mapping consistency. From the magnification in the dotted ellipse in Fig. 13, the robot trajectory in the temporary map is not smooth and contains abrupt displacement, which shows the inconsistency of the temporary map. Note that after the last corner, both trajectories converge to the reference trajectory due to the detection of previously observed landmarks. These landmarks are located around the start position of the robot and they are added to the permanent map with little accumulated errors caused by drifts of odometry. Therefore, after traveling a long loop path, re-observation of these landmarks imposes additional measurement constraints on correction step of EKF algorithm, i.e. (19)-(23), which effectively correct errors accumulated during the SLAM process. We can also see that the trajectory generated from the proposed SLAM algorithm coincides with the ground truth completely, showing much higher accuracy than the standard EKF-SLAM algorithm.

Fig. 14 shows how the estimated position and orientation variance of the robot in the proposed SLAM algorithm vary over time. With more and more new space explored, the uncertainty increases but fluctuates at a reasonable level. After 6000 iterations, the position variance decreases dramatically, which is consistent with the convergence of the robot trajectory in Fig. 13 due to the detection of previously observed landmarks.

The absolute accuracy of the estimated robot position is evaluated only at the end of the SLAM process, by measuring the error of robot position manually. The results are obtained as an average of 10 independent runs, as shown in Table 3. From the results we can clearly draw the conclusion that the robot localization of the proposed SLAM solution is more accurate than that of the standard EKF-SLAM.

TABLE 3. Absolute localization error of robot in two different SLAM algorithms.

Algorithms	Error in x-axis	Error in y-axis
Proposed SLAM algorithm	19 mm	31 mm
Standard EKF-SLAM	107 mm	932 mm

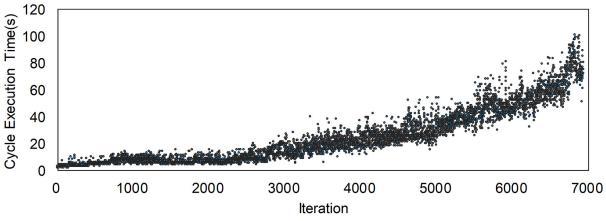

FIGURE 15. Cycle execution time varies during the SLAM process.

Furthermore, the efficiency of the proposed SLAM algorithm is also evaluated in terms of the cycle execution time, since that our SLAM solution mainly aims at practical application in industrial environments. The results in Fig. 15 indicates that the cycle time increases with time, as a result of map size expansion. Overall, the cycle time is maintained at an acceptable level as less than 100ms, which is efficient enough for real time SLAM.

V. CONCLUSIONS

In this paper, a clutter-resistant SLAM solution is developed for AGV in complicated and dynamic industrial environments. The combination of reflector landmarks and line segment landmarks improves the robustness of the SLAM solution. Reflector landmarks make it feasible to employ SLAM solution in many dynamic and complicated industrial scenes, whereas introducing line features extracted from the environments reduces the use of reflector landmarks, thus

lowering operational costs. The proposed reflector recognition method helps distinguishing true reflector landmarks from other clutters, and the dual-map based map management scheme further eliminates all types of fallacious landmarks thoroughly. The effectiveness of these proposed methods is validated through practical experiments. The mapping accuracy, consistency and efficiency are improved by eliminating fallacious landmarks in cluttered environments, which enables accurate and reliable autonomous operation of industrial AGV. These methods can also be employed in other practical scenes such as medical robots, and are suitable for various kinds of landmarks. Our future work will focus on accurate localization of AGV with pre-existing maps in industrial environments.

REFERENCES

[1] X. Xie, Y. Yu, X. Lin, and C. Sun, "An EKF SLAM algorithm for mobile robot with sensor bias estimation," in *Proc. 32nd Youth Academic Annu. Conf. Chin. Assoc. Autom. (YAC)*, May 2017, pp. 281–285.

[2] M. W. M. G. Dissanayake, P. Newman, S. Clark, H. F. Durrant-Whyte, and M. Csorba, "A solution to the simultaneous localization and map building (SLAM) problem," *IEEE Trans. Robot. Autom.*, vol. 17, no. 3, pp. 229–241, Jun. 2001.

[3] K. Zhang, H. Gui, Z. Luo, and D. Li, "Matching for navigation map building for automated guided robot based on laser navigation without a reflector," *Int. J. Robot. Res. Appl.*, vol. 46, no. 1, pp. 17–30, Jan. 2019.

[4] H. Durrant-Whyte and T. Bailey, "Simultaneous localization and mapping: Part I," *IEEE Robot. Autom. Mag.*, vol. 13, no. 2, pp. 99–110, Jun. 2006.

[5] T. Bailey and H. Durrant-Whyte, "Simultaneous localization and mapping (SLAM): Part II," *IEEE Robot. Autom. Mag.*, vol. 13, no. 3, pp. 108–117, Sep. 2006.

[6] A. Chatterjee, O. Ray, A. Chatterjee, and A. Rakshit, "Development of a real-life EKF based SLAM system for mobile robots employing vision sensing," *Expert Syst. Appl.*, vol. 38, no. 7, pp. 8266–8274, Jul. 2011.

[7] R. Koch, S. May, P. Murmann, and A. Nächter, "Identification of transparent and specular reflective material in laser scans to discriminate affected measurements for faultless robotic SLAM," *Robot. Auto. Syst.*, vol. 87, pp. 296–312, Jan. 2017.

[8] R. Yuan, F. Zhang, J. Qu, G. Li, and Y. Fu, "An enhanced pose tracking method using progressive scan matching," *Int. J. Robot. Res. Appl.*, vol. 46, no. 2, pp. 235–246, Mar. 2019.

[9] E. Pedrosa, A. Pereira, and N. Lau, "A non-linear least squares approach to SLAM using a dynamic likelihood field," *J. Intell. Robotic Syst.*, vol. 93, nos. 3–4, pp. 519–532, Mar. 2019.

[10] F. Mastrogiovanni, A. Sgorbissa, and R. Zaccaria, "How the location of the range sensor affects EKF-based localization," *J. Intell. Robotic Syst.*, vol. 68, no. 2, pp. 121–145, Nov. 2012.

[11] G. Klanär, L. Tesliá, and I. Škrjanc, "Mobile-robot pose estimation and environment mapping using an extended Kalman filter," *Int. J. Syst. Sci.*, vol. 45, no. 12, pp. 2603–2618, Dec. 2014.

[12] D. Rodriguez-Losada, F. Matia, L. Pedraza, A. Jimenez, and R. Galan, "Consistency of SLAM-EKF algorithms for indoor environments," *J. Intell. Robotic Syst.*, vol. 50, no. 4, pp. 375–397, Nov. 2007.

[13] G. P. Huang, A. I. Mourikis, and S. I. Roumeliotis, "A quadratic-complexity observability-constrained unscented Kalman filter for SLAM," *IEEE Trans. Robot.*, vol. 29, no. 5, pp. 1226–1243, Oct. 2013.

[14] N. M. Kwok and A. B. Rad, "A modified particle filter for simultaneous localization and mapping," *J. Intell. Robotic Syst.*, vol. 46, no. 4, pp. 365–382, Aug. 2006.

[15] J. Guivant, E. Nebot, and S. Baiker, "Localization and map building using laser range sensors in outdoor applications," *J. Robotic Syst.*, vol. 17, no. 10, pp. 565–583, Oct. 2000.

[16] D. Ribas, P. Ridao, J. Domingo Tardos, and J. Neira, "Underwater SLAM in a marina environment," in *Proc. IEEE/RSJ Int. Conf. Intell. Robots Syst.*, Oct. 2007, pp. 1455–1460.

[17] L. Tesliá, I. Škrjanc, and G. Klanär, "EKF-based localization of a wheeled mobile robot in structured environments," *J. Intell. Robotic Syst.*, vol. 62, no. 2, pp. 187–203, May 2011.

[18] L. Tesliá, I. Škrjanc, and G. Klanär, "Using a LRF sensor in the Kalman-filtering-based localization of a mobile robot," *ISA Trans.*, vol. 49, no. 1, pp. 145–153, Jan. 2010.

[19] M. Quan, S. Piao, M. Tan, and S. Huang, "Accurate monocular visual-inertial slam using a map-assisted ekf approach," *IEEE Access*, vol. 7, pp. 34,289–34300, 2019.

[20] M. N. Santhanakrishnan, J. B. B. Rayappan, and R. Kannan, "Implementation of extended Kalman filter-based simultaneous localization and mapping: A point feature approach," *Sādhanā*, vol. 42, no. 9, pp. 1495–1504, Sep. 2017.

[21] Y. Zhang, T. Zhang, and S. Huang, "Comparison of EKF based SLAM and optimization based SLAM algorithms," in *Proc. 13th IEEE Conf. Ind. Electron. Appl. (ICIEA)*, May 2018, pp. 1308–1313.

[22] B. Triggs, P. McLauchlan, R. Hartley, and A. Fitzgibbon, "Bundle adjustment—A modern synthesis," in *Vision Algorithms: Theory and Practice*, B. Triggs, A. Zisserman, and R. Szeliski, Eds. Berlin, Germany: Springer, 2000, pp. 298–372.

[23] F. Lu and E. Milios, "Globally consistent range scan alignment for environment mapping," *Auto. Robots*, vol. 4, no. 4, pp. 333–349, 1997.

[24] M. W. Mehrez, G. K. I. Mann, and R. G. Gosine, "An optimization based approach for relative localization and relative tracking control in multi-robot systems," *J. Intell. Robot. Syst.*, vol. 85, no. 2, pp. 385–408, Feb. 2017.

[25] C. Chen and H. Zhu, "Visual-inertial SLAM method based on optical flow in a GPS-denied environment," *Ind. Robot, Int. J.*, vol. 45, no. 3, pp. 401–406, May 2018.

[26] Z. Wang, Q. Zhang, J. Li, S. Zhang, and J. Liu, "A computationally efficient semantic SLAM solution for dynamic scenes," *Remote Sens.*, vol. 11, no. 11, p. 1363, Jun. 2019.

[27] L. Zhao, Z. Liu, J. Chen, W. Cai, W. Wang, and L. Zeng, "A compatible framework for RGB-D SLAM in dynamic scenes," *IEEE Access*, vol. 7, pp. 75604–75614, 2019.

[28] L. Sun, F. Kanehiro, I. Kumagai, and Y. Yoshiyasu, "Multi-purpose SLAM framework for dynamic environment," in *Proc. IEEE/SICE Int. Symp. Syst. Integr. (SII)*, Jan. 2020, pp. 519–524.

[29] Y. Sun, M. Liu, and M. Q.-H. Meng, "Improving RGB-D SLAM in dynamic environments: A motion removal approach," *Robot. Auton. Syst.*, vol. 89, pp. 110–122, Mar. 2017.

[30] C. Sheng, S. Pan, P. Zeng, L. Huang, and T. Zhao, "Monocular slam system in dynamic scenes based on semantic segmentation," in *Proc. Int. Conf. Image Graph.* Cham, Switzerland: Springer, 2019, pp. 593–603.

[31] Y. Ai, T. Rui, M. Lu, L. Fu, S. Liu, and S. Wang, "DDL-SLAM: A robust RGB-D SLAM in dynamic environments combined with deep learning," *IEEE Access*, early access, Apr. 30, 2020, doi: 10.1109/ACCESS.2020.2991441.

[32] M. Dymczyk, E. Stumm, J. Nieto, R. Siegwart, and I. Gilitschenski, "Will it last? Learning stable features for long-term visual localization," in *Proc. 4th Int. Conf. 3D Vis. (3DV)*, Oct. 2016, pp. 572–581.

[33] F. Demim, A. Nemra, A. Boucheloukh, E. Kobzili, M. Hamerlain, and A. Bazoula, "SLAM based on adaptive SVSF for cooperative unmanned vehicles in dynamic environment," *IFAC-PapersOnLine*, vol. 52, no. 8, pp. 73–80, 2019.

[34] F. Demim, A. Boucheloukh, A. Nemra, E. Kobzili, M. Hamerlain, and A. Bazoula, "An adaptive SVSF-SLAM algorithm in dynamic environment for cooperative unmanned vehicles," *IFAC-PapersOnLine*, vol. 52, no. 15, pp. 394–399, 2019.

[35] A. Vakhitov and V. Lempitsky, "Learnable line segment descriptor for visual slam," *IEEE Access*, vol. 7, pp. 39923–39934, 2019.

[36] R. Gomez-Ojeda, F.-A. Moreno, D. Zuniga-Noel, D. Scaramuzza, and J. Gonzalez-Jimenez, "PL-SLAM: A stereo SLAM system through the combination of points and line segments," *IEEE Trans. Robot.*, vol. 35, no. 3, pp. 734–746, Jun. 2019.

[37] R. Wang, Y. Wang, W. Wan, and K. Di, "A point-line feature based visual SLAM method in dynamic indoor scene," in *Proc. Ubiquitous Positioning, Indoor Navigat. Location-Based Services (UPINLBS)*, Mar. 2018, pp. 1–6.

[38] J. Seong, J. Kim, and W. Chung, "Mobile robot localization using indistinguishable artificial landmarks," in *Proc. 10th Int. Conf. Ubiquitous Robots Ambient Intell. (URAI)*, Oct. 2013, pp. 222–224.

[39] T. Nakamura and S. Suzuki, "Simplified slam using reflection intensity of laser range sensor with retro-reflective marker," in *Proc. SICE Annu. Conf. (SICE)*, 2012, pp. 2074–2079.

[40] S. Thrun, W. Burgard, and D. Fox, *Probabilistic Robotics*. Cambridge, MA, USA: MIT Press, 2005.

[41] V. Nguyen, S. Gächter, A. Martinelli, N. Tomatis, and R. Siegwart, "A comparison of line extraction algorithms using 2D range data for indoor mobile robotics," *Auto. Robots*, vol. 23, no. 2, pp. 97–111, Aug. 2007.
[42] G. Li, J. Meng, Y. Xie, X. Zhang, L. Jiang, and Y. Huang, "An improved observation model for monte-carlo localization integrated with reliable reflector prediction," in *Proc. IEEE/ASME Int. Conf. Adv. Intell. Mechatronics (AIM)*, Jul. 2019, pp. 972–977.
[43] M. Hu, H. Ao, and H. Jiang, "Experimental research on feature extraction of laser SLAM based on artificial landmarks," in *Proc. Chin. Control Decis. Conf. (CCDC)*, Jun. 2019, pp. 5495–5500.
[44] J. Neira and J. D. Tardos, "Data association in stochastic mapping using the joint compatibility test," *IEEE Trans. Robot. Autom.*, vol. 17, no. 6, pp. 890–897, 2001.

WEI WANG was born in Anqing, China, in 1993. He received the B.E. degree in logistics engineering from Shandong University, Jinan, China, in 2015. He is currently pursuing the Ph.D. degree with the School of Control Science and Engineering, Shandong University, and has spent one year studying in the School of Industrial Systems and Engineering, Georgia Institute of Technology. His research interests are mainly focused on mobile robots and robotics systems.

YAOHUA WU received the M.E. degree from Shandong University, Jinan, in 1991, and the Ph.D. degree in mechanical engineering from Tsinghua University, Beijing, China, in 1996. He is currently a Professor with the School of Control Science and Engineering, and also the Head of the Modern Logistics Research Center, Shandong University. His research interests include automated logistics system, autonomous logistics devices, and logistics software design.

ZHENYU JIANG was born in Qingdao, China, in 1993. He received the M.E. degree from Shandong University. He is currently pursuing the Ph.D. degree with Tsinghua University. His fields of research interests are logistics engineering and supply chain management.

JIAHUI QI was born in Shenyang, China, in 1994. He received the B.E. degree from Northeastern University. He is currently pursuing the master's degree with the School of Control Science and Engineering, Shandong University. His fields of research interests are localization and trajectory tracking control of mobile robots.